Pamoic acid is an inhibitor of HMGB1•CXCL12 elicited chemotaxis and reduces inflammation in murine models of Pseudomonas aeruginosa pneumonia

Federica De Leo
Universita Vita Salute San Raffaele
Alice Rossi
San Raffaele Institute: IRCCS Ospedale San Raffaele
Francesco De Marchis
Universita Vita Salute San Raffaele
Cristina Cigana
San Raffaele Institute: IRCCS Ospedale San Raffaele
Mededе Melessike
San Raffaele Institute: IRCCS Ospedale San Raffaele
Giacomo Quilici
San Raffaele Institute: IRCCS Ospedale San Raffaele
Ida De Fino
San Raffaele Institute: IRCCS Ospedale San Raffaele
Malisa Vittoria Mantonico
Universita Vita Salute San Raffaele
Chantal Fabris
San Raffaele Institute: IRCCS Ospedale San Raffaele
Alessandra Bragonzi
San Raffaele Institute: IRCCS Ospedale San Raffaele
Marco Emilio Bianchi
Vita-Salute San Raffaele University: Universita Vita Salute San Raffaele
Giovanna Musco (musco.giovanna@hsr.it)
Universita Vita e Salute San Raffaele: Universita Vita Salute San Raffaele https://orcid.org/0000-0002-0469-2994

Research Article

Keywords: HMGB1, CXCL12, inflammation, Pseudomonas aeruginosa, efficacy-testing, respiratory infection, mouse model.

Posted Date: April 14th, 2022

DOI: https://doi.org/10.21203/rs.3.rs-1536525/v1

Pamoic acid is an inhibitor of HMGB1•CXCL12 elicited chemotaxis and reduces inflammation in murine models of *Pseudomonas aeruginosa* pneumonia

Federica De Leo[1,2*], Alice Rossi[3*], Francesco De Marchis[3], Cristina Cigana[3], Medede Melessike[3], Giacomo Quilici[1], Ida De Fino[3], Malisa V. Mantonico[1,2], Chantal Fabris[1], Alessandra Bragonzi[3§], Marco E. Bianchi[2§], Giovanna Musco[1§]

[1]Biomolecular NMR Laboratory, Division of Genetics and Cell Biology, IRCCS San Raffaele Scientific Institute, Milano, Italy

[2]Università Vita e Salute-San Raffaele, Milano

[3]Infection and Cystic Fibrosis Unit, Division of Immunology, Transplantation and Infectious Diseases, IRCCS San Raffaele Scientific Institute, Milano, Italy

*Co-first authors

[§]To whom correspondence should be addressed: bragonzi.alessandra@hsr.it, bianchi.marco@hsr.it, musco.giovanna@hsr.it

Running title: Pharmacological inhibition of HMGB1 in *Pseudomonas aeruginosa* pneumonia

Keywords: HMGB1, CXCL12, inflammation, *Pseudomonas aeruginosa*, efficacy-testing, respiratory infection, mouse model.

This article has Supplementary Information.

Abstract

Background. High-mobility group box 1 protein (HMGB1) is an ubiquitous nuclear protein that once released in the extracellular space acts as a Damage Associated Molecular Pattern and promotes inflammation. HMGB1 is significantly elevated during *Pseudomonas aeruginosa* infections and has a clinical relevance in respiratory diseases such as Cystic Fibrosis (CF). Salicylates are HMGB1 inhibitors. To address pharmacological inhibition of HMGB1 with small molecules, we explored the therapeutic potential of pamoic acid (PAM), a salicylate with limited ability to cross epithelial barriers.

Methods. PAM binding to HMGB1 and CXCL12 was tested by Nuclear Magnetic Resonance Spectroscopy using chemical shift perturbation methods, and inhibition of HMGB1•CXCL12–dependent chemotaxis was investigated by cell migration experiments. Aerosol delivery of PAM, with single or repeated administrations, was tested in murine models of acute and chronic *P. aeruginosa* pulmonary infection in C57Bl/6NCrlBR mice. PAM efficacy was evaluated by read-outs including weight loss, bacterial load and inflammatory response in lung and bronco-alveolar lavage fluid.

Results. Our data and three-dimensional models show that PAM is a direct ligand of both HMGB1 and CXCL12. We also showed that PAM is able to interfere with heterocomplex formation and the related chemotaxis *in vitro*. Importantly, PAM treatment by aerosol was effective in reducing acute and chronic airway murine inflammation and damage induced by *P. aeruginosa*. The results indicated that PAM reduces leukocyte recruitment in the airways, in particular neutrophils, suggesting an impaired in vivo chemotaxis. This was associated with a decrease in myeloperoxidase and neutrophil elastase levels. Modestly increased bacterial burdens

were recorded with single administration of PAM in acute infection; however, repeated administration in chronic infection did not affect bacterial burdens, indicating that the interference of PAM with the immune system has a limited risk of pulmonary exacerbation.

Conclusions. This work established the efficacy of treating inflammation in chronic respiratory diseases, including bacterial infections, by topical delivery in the lung of PAM, an inhibitor of HMGB1.

Background

High-mobility group box 1 protein (HMGB1) is a highly conserved and ubiquitous nuclear protein (215 amino acids) that acts as a Damage Associated Molecular Pattern promoting inflammation when released in the extracellular space and alarms the immune system. Excessive release of HMGB1 may mediate the systemic inflammatory response syndrome. Immune cells secrete HMGB1 in response to a variety of stimuli, such as pathogen associated molecular patterns (e.g. lipopolysaccharide) and bacterial infections (Lu et al. 2014). Accordingly, high levels of HMGB1 as well as negative correlation between HMGB1 levels and lung function have been described in the context of chronic respiratory diseases, such as chronic obstructive pulmonary disease (COPD) and cystic fibrosis (CF) (Chirico et al. 2015; Gangemi et al. 2015; Liou et al. 2012). Moreover, HMGB1 levels are predictive of time-to-first acute pulmonary exacerbation (APE), number of future APEs within five years and time-to-lung transplantation or death in CF patients (Liou et al. 2012). High secretion of HMGB1 has been also observed during *Pseudomonas aeruginosa* infections, such as those associated with COPD and CF, with significant high concentrations in the sputum of CF patients (Liou et al. 2012; Rowe et al. 2008).

Once released by infected epithelial cells, HMGB1 orchestrates responses to tissue damage recruiting neutrophils and impairing bacterial clearance (Bianchi et al. 2017).

Recruitment of inflammatory cells to damaged tissues after infection or injury relies on the interaction of the fully reduced form of HMGB1 with the chemokine C-X-C Motif Chemokine Ligand 12 (CXCL12). The HMGB1•CXCL12 complex in turn promotes C-X-C chemokine receptor type 4 (CXCR4)-dependent recruitment of inflammatory cells to injured tissues (Schiraldi et al. 2012), which exacerbates the immune response in pathological conditions (D'Agostino et al. 2018).

Notably, during *P. aeruginosa* infection neutralization of HMGB1 in the lung with monoclonal antibodies resulted in significant protection, with reduction of neutrophil recruitment and lung injury in both *cystic fibrosis transmembrane conductance regulator* deficient ($Cftr^{-/-}$) and wild-type mice (Entezari et al. 2012). However, effective, systemic intraperitoneal (i.p.) delivery of monoclonal antibodies would be expensive and impractical for chronic treatments. Hence, the pharmacological targeting of HMGB1 with small molecules could be a valuable alternative in the treatment of inflammation in chronic respiratory diseases and in pulmonary bacterial infections. In the past, we have shown that HMGB1 is druggable with small molecules such as glycyrrhizin (Mollica et al. 2007) and salicylates: salicylic acid (Choi et al. 2015), Diflunisal (De Leo et al. 2019), 5,5′-Methylenedi-2,3-Cresotic Acid (MCA) (De Leo et al. 2020). All these molecules inhibit HMGB1 chemoattractant activity through the disruption of its heterocomplex with CXCL12 (HMGB1●CXCL12) and impairment of the HMGB1/CXCL12/CXCR4 axis.

We then asked whether other salicylates could effectively inhibit the detrimental HMGB1 activity in bacterial pulmonary infections. We focused our attention on pamoic acid (PAM), a solubilizer commonly used in drug formulations and which is not absorbed across mucosae and

by the oral route (Neubig 2010; Zhao et al. 2010). We show here that PAM directly binds to both HMGB1 and CXCL12, disrupts their heterocomplex, herewith inhibiting HMGB1•CXCL12 dependent chemotaxis *in vitro*. Importantly, PAM delivered by aerosol *in vivo* to C57BL/6NCrlBR mice with *P. aeruginosa* infection shows no toxicity in the airways and can ameliorate neutrophilic inflammation and lung damage.

These results show for the first time a promising efficacy of a small molecule inhibitor of HMGB1-dependent inflammation in mouse models of acute and chronic *P. aeruginosa* respiratory infection.

Materials and Methods

Ethics Statement. Animal studies adhered strictly to the Italian Ministry of Health guidelines for the use and care of experimental animals (protocol #733). Research with the *P. aeruginosa* multidrug-resistant (MDR)-RP73 isolate from a CF individual and storage of biological materials were approved by the Ethics Commission of Hannover Medical School, Germany.

Proteins Expression and Purification

Recombinant HMGB1 constructs (Accession code P63158, residues 1-215 and BoxA, residues 1–89) and recombinant human CXCL12 in labeled and unlabeled forms were produced as described in (De Leo et al. 2019). Proteins used for cell-based assays were provided by HMGBiotech (Milan). Pamoic acid was purchased from Sigma Aldrich.

Nuclear Magnetic Resonance (NMR) experiments.

After expression and purification, HMGB1 was dialyzed against NMR buffer, containing 20 mM phosphate buffer pH 7.3, 150 mM NaCl, and 1 mM DTT. CXCL12 was dialyzed against a buffer containing 20 mM phosphate buffer pH 6, 20 mM NaCl. Protein concentrations were determined considering molar extinction coefficients at 280 nm of 21430 and 8700 M^{-1} cm^{-1} for HMGB1 and CXCL12, respectively. NMR spectra were recorded at 298K on a Bruker Avance 600 MHz spectrometer (Karlsruhe, Germany) equipped with a triple-resonance TCI cryoprobe with an x, y, z-shielded pulsed-field gradient coil. Spectra were processed with TopspinTM 3.2 (Bruker) and analyzed with CcpNmr Analysis 2.4 (Vranken et al. 2005). Details on PAM resonance assignments, on Saturation Transfer Difference (STD) and Water-Ligand Observed via Gradient Spectroscopy (WaterLOGSY) experiments, on NMR titrations and on line-shape analysis are reported in Supplementary information.

Data Driven Docking Models and molecular images.

Molecular docking of PAM on CXCL12 (PDB 4UAI), on BoxA (residues G3-Y77) and on BoxB (A93-G173), whose structures were extracted from 2YRQ (first structure of the NMR bundle), were performed using the data-driven docking software HADDOCK 2.2 (Dominguez et al. 2003; Van Zundert et al. 2016) and following the classical three-stage procedure, which includes: (1) randomization of orientations and rigid body minimization, (2) simulated annealing in torsion angle space, and (3) refinement in Cartesian space with explicit water. Details on docking calculations, Ambiguous interaction restraints (AIRs) and cluster analysis are reported in Supplementary information.

Molecular images were generated by 3D Protein Imaging online server (Tomasello et al. 2020). CSP plots were produced with Xmgrace program (http://plasma-gate.weizmann.ac.il/Grace/).

Cell Migration Experiments.

For fibroblast chemotaxis, modified Boyden chambers were used with filters (pore diameter 8μm; Neuro Probe) coated with 50 μg/mL fibronectin (Roche). Mouse 3T3 cells (50,000 in 200 μL) were added to the upper chamber. Serum-free DMEM as negative control, HMGB1, and/or PAM were added to the lower chamber at the indicated concentrations, and then cells were left to migrate for 3h at 37 °C. Cells were fixed with ethanol and stained with Giemsa Stain (Sigma), then non-migrating cells were removed with a cotton swab. All assays were done at least in biological triplicate and were repeated at least twice. The migrated cells were acquired with Zeiss Imager M.2 microscope at 10x magnification, then evaluated with an automated counting program.

Mouse models of acute and chronic *P. aeruginosa* infection.

P. aeruginosa strains included PAO1 and MDR-RP73 strains isolated from a CF patient's airways. Immunocompetent C57Bl/6NCrlBR male mice (8-10 weeks, Charles River Calco, Italy) were challenged with $1x10^6$ colony-forming units (CFUs) of the planktonic PAO1 strain for acute infection or with 5×10^5 CFUs of the MDR-RP73 strain embedded in agar beads for chronic infection by intratracheal inoculation (i.t.), as previously described (Bragonzi et al. 2009; Cigana et al. 2016; Facchini et al. 2014). Mice were treated with PAM (1 mM and 3 mM) or vehicle (PBS) by local pulmonary administration using the Penn-Century MicroSprayer® Aerosolizer with treatment schedules established previously (Cigana et al. 2020). In the acute infection

158 model, the treatment schedule used with PAM was a single dose administered after infection. In
159 the chronic infection model daily doses repeated for seven days were administered. Body weight
160 and health status were monitored daily. CFU counts, and cell counts in the bronchoalveolar
161 lavage fluid (BALF) were analyzed as previously described (Cigana et al. 2016; Facchini et al.
162 2014; Kukavica-Ibrulj et al. 2014) at six hours after acute infection or seven days after chronic
163 infection. Myeloperoxidase (MPO) and neutrophil elastase were measured in the BALF and lung
164 homogenates by ELISA (R&D DuoSet ELISA Development System). Additional details in
165 accordance with the Animal Research: Reporting of In Vivo Experiments guidelines (Kilkenny
166 et al. 2010) are reported in Supplementary material.
167
168 **Statistics.** Statistical analyses were performed with GraphPad Prism using one-way ANOVA
169 plus Dunnett's post-test for *in vitro* data, two-way ANOVA with Bonferroni Multiple
170 Comparison test for body weight change and temperature and Kruskal-Wallis test with Dunn's
171 Multiple Comparison test for the other *in vivo* readouts.
172
173 **Results**
174 **PAM binds HMGB1 and CXCL12 and inhibits the HMGB1•CXCL12 heterocomplex *in***
175 ***vitro*.**
176 To investigate whether PAM is a direct ligand of HMGB1 we first used a battery of Nuclear
177 Magnetic Resonance (NMR) binding experiments including Saturation Transfer Difference
178 (STD), Water-Ligand Observed via Gradient SpectroscopY (waterLOGSY) and chemical shift
179 perturbation (CSP). STD effects, inversion of the sign in waterLOGSY spectra and overall line
180 broadening effects of PAM (1 mM) in the presence of 50 μM HMGB1 first indicated a protein-

ligand interaction (**Supplementary Figure S1**). NMR titrations of ^{1}H-^{15}N labeled HMGB1 with PAM confirmed binding, with a specific set of amide resonances significantly shifting (CSP > Avg+SD) or disappearing upon addition of increasing concentrations of PAM (up to 0.1 mM) (**Supplementary Figure S2)**. Residues whose amides were mostly affected by the binding (R9, G10, A16, F17, Q20, T21, R23, S45, F104, R109, G122, D123) when mapped on BoxA and BoxB structures (**Figure 1A**) defined a small pocket on the short arm of the L-shaped fold of both HMG boxes (**Figure 1A**). This interaction surface was well in line with the one previously reported for other HMGB1 inhibitors (De Leo et al. 2019). The binding occurred in the fast-intermediate exchange regime on the NMR time scale, in agreement with the apparent K_d of 170 ± 17 μM obtained by lineshape analysis of the peaks in ^{1}H-^{15}N HSQC spectra as a function of added ligand (Waudby et al. 2016). The residues with significant CSPs were then used to generate three-dimensional data-driven docking models of PAM in complex with BoxA and BoxB (**Figure 1A**). Both models highlighted a central clamping electrostatic interaction between the PAM carboxylate and the guanidinium groups of R23 and R109 on BoxA and BoxB, respectively. The interaction was further stabilized by van der Waals (vdW) contacts between the aromatic rings of PAM and the hydrophobic sidechains of residues on BoxA (F17, F18, V19, V35) and BoxB (F104, V124, A125) (**Figure 1A, Supplementary Figure S3, S4**). The models agreed with the ligand epitope mapping *via* STD buildup experiments and intermolecular Nuclear overhauser effects (NOEs), that indicated proximity between the aromatic protons of PAM (H2, H3 and H4) and HMGB1 (**Supplementary Figure S5, and Table S1**).

We have recently shown that HMGB1 ligands often interact with CXCL12. Indeed, NMR titrations of ^{15}N-CXCL12 with PAM indicated binding (apparent K_d of 66 ± 4 μM), with significant CSPs affecting residues V23, K24, H25, L26, K27, Q48, V49 (**Figure 1B,**

Supplementary Figure S6). A data-driven docking model suggested that PAM, similarly to diflunisal and MCA (De Leo et al. 2020; De Leo et al. 2019), binds in the so-called CXCR4 sulfotyrosine (sulfoY21) binding site (Veldkamp et al. 2008). The PAM carboxylate establishes polar interactions with the amide side chains of N44 and N45, the hydroxyl group creates an H-bond with the guanidinium group of R47, the second carboxylate has polar interactions with Q48 backbone atoms, and the aromatic rings establish stabilizing hydrophobic interactions with V49 and V18 (**Figure 1B, Supplementary Figure S7**).

Next, by NMR-based Antagonist Induced Dissociation Assay (Krajewski et al. 2007) we proved that PAM disrupts the HMGB1•CXCL12 heterocomplex. We acquired ^{15}N HSQC spectra of the free ^{15}N-HMGB1 (**Figure 1C** black contours) and of a preformed complex of ^{15}N-HMGB1 (0.1 mM) with unlabeled CXCL12 (0.2 mM) (**Figure 1C** red contours). The latter displayed evident line broadening and reduction of the ^{15}N-HMGB1 peaks (**Figure 1C**) due to the complex intermediate exchange regime on the NMR time scale (De Leo et al. 2019). The addition of a sub-stoichiometric amount of PAM reduced the line broadening effect and recovered the ^{1}H-^{15}N resonances in the ^{1}H-^{15}N HSQC spectrum of HMGB1, indicating that the complex was partially disrupted.

Collectively these data indicate that PAM is a direct ligand of both HMGB1 and CXCL12 and is able to interfere with heterocomplex formation.

PAM inhibits HMGB1•CXCL12 dependent chemotaxis

Next, we asked whether PAM was able to inhibit the chemotaxis elicited by HMGB1 and by the HMGB1•CXCL12 heterocomplex. Indeed PAM reduced the HMGB1-dependent migration of 3T3 mouse fibroblasts in a dose-dependent way with an IC_{50} of about 30 nM (**Figure 2A**). The

inhibition of HMGB1 chemotactic activity was specific, as PAM did not affect chemotaxis toward fMLP (**Figure 2A**). As expected, PAM also inhibited chemotaxis induced by HMGB1•CXCL12 (**Figure 2B**). Taken together these data indicate that PAM is a very effective inhibitor of the chemotactic activity HMGB1•CXCL12 heterocomplex *in vitro*.

PAM reduces inflammation and tissue damage in a murine model of acute *P. aeruginosa* pneumonia

Since PAM inhibits *in vitro* the HMGB1•CXCL12 elicited chemotaxis, we asked whether it could impair neutrophil recruitment in a murine model of acute *P. aeruginosa* respiratory infection (Bragonzi 2010; Cigana et al. 2020). First, we tested toxicity in C57BL/6NCrlBR mice with two different doses (1 and 3 mM) of PAM by aerosol in repeated daily administrations for 7 days. Several readouts including weight loss, body temperature and health status after treatment did not show significant changes between PAM and vehicle (**Supplementary S8A** and data not shown). Next, C57BL/6NCrlBR mice were challenged with planktonic *P. aeruginosa* PAO1 strain by i.t. inoculation to induce acute infection. Local treatment *via* the aerosol route with 1 and 3 mM PAM started five minutes after infection and was compared with vehicle (PBS). To define the effect of PAM on the airway inflammatory response, we measured leukocyte recruitment in the BALF six hours after infection. A single dose of PAM reduced total cells, particularly neutrophils in a dose-dependent manner with statistical significance at 3 mM PAM compared to vehicle (**Figure 3A and B**). No significant difference was observed in macrophage numbers (**Figure 3C**). Next, MPO and neutrophil elastase, markers of neutrophil infiltration and tissue damage (Haegens et al. 2008), were measured by ELISA. MPO levels in BALF and lung were significantly reduced in mice treated with 3 mM PAM compared to vehicle (**Figure 3D**

and E). Conversely, neutrophil elastase both in BALF and lung supernatant was not affected by PAM treatment (**Supplementary S9A and B**). When bacterial burdens in the lung were evaluated, moderately but significantly higher CFUs were found in mice treated with 3 mM PAM in comparison to those treated with vehicle (**Figure 3F**). No difference in the CFUs was observed between 1 mM PAM and vehicle. Our results indicate that a single dose of PAM treatment by aerosol was effective in reducing acute airway murine inflammation and damage induced by *P. aeruginosa* in a dose dependent manner. However, PAM efficacy was associated with a modest increase in bacterial burden, indicating a low risk of acute pulmonary exacerbation in this murine model.

PAM reduces inflammatory response but controls bacterial burden in a mouse model of chronic *P. aeruginosa* pneumonia

Next, we tested the efficacy of repeated doses of PAM in treating chronic lung infections.

To mimic a chronic infection, mice received i.t. inoculations of the *P. aeruginosa* MDR-RP73 strain embedded in agar beads (Facchini et al. 2014). Administration via the aerosol route with 1 mM, 3 mM PAM or vehicle (PBS) was started five minutes after infection and was repeated daily for seven administrations. Over the course of 7 days, mice treated with 3 mM PAM exhibited less loss and faster recovery of body weight than vehicle-treated mice (**Figure 4A**). No significant differences in bacterial load were observed after treatment with PAM (1 and 3 mM) or vehicle, indicating that this schedule of treatment does not affect the chronic *P. aeruginosa* infection (**Figure 4B**).

Treatment with 3 mM PAM reduced the total cell counts (**Figure 4C)** with significant difference in the number of neutrophils in BALF when compared to vehicle, indicating a reduction of

inflammation (**Figure 4D**). No differences were observed in the number of macrophages (**Figure 4E**). Cellular recruitment in mice treated with 1 mM PAM followed the same trend, but differences with vehicle did not reach statistical significance. Next, to validate these results, MPO levels and neutrophils elastase in BALF and lung supernatant were measured. Neutrophils elastase levels in BALF supernatant were significantly reduced in mice treated with 3 mM PAM compared to vehicle (**Figure 4F).** No difference in neutrophil elastase were observed in the supernatant of lung homogenate after PAM treatment (**Supplementary Figure S10C**). MPO levels were similar in PAM treated mice compared to vehicle (**Supplementary Figure S10A and B**). Our results indicate that repeated doses of PAM treatment by aerosol were effective in reducing chronic airway murine inflammation induced by *P. aeruginosa* in a dose dependent manner without affecting bacterial burden.

DISCUSSION

Increasing evidences suggest that inhibition of the alarmin HMGB1 in *P. aeruginosa* infection could offer a potential therapeutic strategy to reduce bacterial infection and lung inflammation. Previous research showed that delivery of monoclonal antibodies (mAB) against HMGB1 conferred significant protection against *P. aeruginosa* infection, neutrophil recruitment and lung injury in mouse models of CF (Entezari et al. 2012). In addition, delivery of recombinant BoxA, an HMGB1 antagonist, is effective in reducing Toll like receptor 4 (TLR4), Receptor for advanced glycation (RAGE), and inflammatory cytokines levels in the cornea of *P. aeruginosa*-infected mice (Ekanayaka et al. 2018).

Importantly, recent work in our groups has also shown that HMGB1 is druggable and that its ability to recruit immune cells upon injury can be modulated by small molecules (De Leo et al.

2020; De Leo et al. 2019), a strategy that appears more convenient than inhibition through mAb or biologics. In particular, salicylates appear to be well suited in impairing the HMGB1•CXCL12 heterocomplex, through direct targeting of both HMGB1 and CXCL12; they effectively inhibit chemotaxis *via* the HMGB1/CXCL12/CXCR4 axis (De Leo et al. 2020; De Leo et al. 2019). During a structure-activity relationship study aiming at identifying salicylate derivatives with improved HMGB1 inhibition activity, we were intrigued by the physical-chemical properties of PAM (Nazir et al. 2019). This molecule (also known as Embonic Acid) does not cross lipid membranes and cannot traverse mucosal barriers, and is thus well-suited for aerosol local delivery. Importantly, PAM is already used in drug formulations (Chue and Chue 2012; Song et al. 2016) and might therefore benefit from a fast track for approval by regulatory agencies.

Here we have shown that PAM, similarly to other salicylates, is a direct ligand of both HMGB1 and CXCL12. The pattern of interaction of PAM with the single HMG Boxes and with CXCL12 is highly reminiscent of the one observed for Diflunisal (De Leo et al. 2019) and MCA (De Leo et al. 2020). PAM appears appropriate to interact with both HMG boxes, as it fulfills three out of the four pharmacophoric requirements previously defined for HMGB1 ligands, consisting of two hydrophobic and two H-bonding acceptor features (De Leo et al. 2020). In particular, data driven docking models indicate that major interactions between the ligand and the target consist of a salt bridge between one carboxylate of PAM and the guanidinium groups of the conserved R23 and R109, and hydrophobic interactions between the naphthalene ring and the hydrophobic patch at the interface of the two helices forming the short arm of the L-shaped HMG boxes.

Moreover, PAM interacts with CXCL12 accommodating in the CXCR4 sulfoY21 binding site (Veldkamp et al. 2008), with its two salicylate moieties establishing polar interactions with R47, N44, and N45 side chains and with the backbone amide of Q48.

Importantly, in strong analogy to the other known HMGB1 ligands (including glycyrrhizin, Diflunisal and MCA), PAM inhibits HMGB1•CXCL12 heterocomplex formation and the heterocomplex-mediated chemotaxis (IC_{50} = 30 nM).

Prompted by these *in vitro* results, we explored the therapeutic potential of PAM and used it both in the acute infection model established by direct intratracheal administration of the planktonic reference strain PAO1 and the chronic infection model established by the clinical MDR-RP73 strain embedded in agar beads (Bragonzi 2010; Cigana et al. 2020; Facchini et al. 2014; Kukavica-Ibrulj et al. 2014). Direct instillation by aerosol was preferred for local delivery of PAM as therapeutic agent into murine lung. Toxicity study showed no adverse effect for PAM up to 3mM. In the acute infection model, PAM substantially reduced the inflammatory profile in the airways, particularly the neutrophil load, induced by *P. aeruginosa.* This is also strengthened by decreased MPO levels in different pulmonary districts including BALF and lung. This may reflect the contribution of immunomodulatory effects inhibiting HMGB1•CXCL12 dependent chemotaxis as suggested by *in vitro* data.

Previous studies in humans and murine models, including those from our group (Döring et al. 2014), have shown that therapeutic strategies that interfere with innate immune recruitment mechanisms have to be implemented with great caution since they harbor the risk of disabling innate host defense mechanisms and favoring risk of sepsis. Considering the potential interference of PAM with innate immune recruitment mechanisms, we evaluated the possible risk of favoring bacterial infections. In the acute infection model, PAM efficacy was associated with a modest increased bacterial burden, indicating a low risk of acute pulmonary exacerbation in a single-dose treatment. Next, we used a chronic infection model to evaluate whether PAM was still effective in a different dynamic of cell mediated immunity and disease progression. We

used the reported long-term chronic pulmonary infection murine model established previously to recapitulate the lung pathology of CF patients (Cigana et al. 2016). In chronic model, mice treated by local (aerosol) repeated administration of PAM early after infection exhibited increased recovery and gain of body weight, compared to vehicle-treated animals, indicating improved health conditions. PAM was effective in reducing chronic airway murine inflammation induced by *P. aeruginosa* in a dose dependent manner, confirming results obtained in the acute infection model. In addition, PAM reduced also neutrophilic elastase suggesting limited tissue damage. Most importantly, the immunomodulator activity of PAM did not affect bacterial burden indicating that this regimen does not exacerbate the infection.

Overall, we have been able to establish the efficacy of PAM as a new small molecule with anti-inflammatory activity and the window of treatment opportunity in *P. aeruginosa* infection. This is of particular importance in chronic infection, as in patients with CF, since administration of compounds which interfere with the immune system may increase the risk of pulmonary exacerbation (Döring et al. 2014). Our anti-inflammatory approach might also cooperate with co-treatments with antibiotics and/or mucolytics and/or CFTR modulators. PAM might be effective in CF patients with a mutation-agnostic/unknown profile. More studies are required, yet these results are good premises for the use of small molecule PAM in inflammatory pulmonary diseases, including COVID-19, where extracellular HMGB1 is expected to play a crucial role (Andersson et al. 2020).

List of abbreviations: bronchoalveolar lavage fluid (BALF), cystic fibrosis (CF), colony-forming units (CFUs), cystic fibrosis transmembrane conductance regulator (CFTCR), chronic obstructive pulmonary disease (COPD), chemical shift perturbation (CSP), C-X-C Motif

Chemokine Ligand 12 (CXCL12), High Mobility Group B1 (HMGB1), heteronuclear single quantum coherence (HSQC), pamoic acid (PAM), Myeloperoxidase (MPO), Nuclear Magnetic Resonance (NMR), Nuclear overhauser effect (NOE), Receptor for advanced glycation (RAGE), Saturation Transfer Difference (STD), Toll like receptor 4 (TLR4), water-Ligand Observed via Gradient SpectroscopY (waterLOGSY),

Ethics Statement

Animal studies adhered strictly to the Italian Ministry of Health guidelines for the use and care of experimental animals (protocol #733). Research with the *P. aeruginosa* multidrug-resistant (MDR)-RP73 isolate from a CF individual and storage of biological materials were approved by the Ethics Commission of Hannover Medical School, Germany.

Availability of data and materials

The datasets used and/or analyzed during the current study are available from the corresponding author on reasonable request.

Competing interests

The authors declare that they have no conflict of interest. However, M.E.B. is founder and part-owner of HMGBiotech, a company that provides goods and services related to HMGB proteins**.**

Funding

The research leading to these results has received funding from Italian Cystic Fibrosis Research Foundation (FFC#22/2018 to M.E.B. and CFaCore to A.B.), with the contribution of the

388 Delegazione FFC di Pesaro; from AIRC under IG 2018 - ID. 21440 project, P.I. G.M., from
389 Fondazione Veronesi (to FDL).

390

391 **Acknowledgements**

392 The authors would like to thank B. Tümmler (Hannover Medical School, Hannover, Germany)
393 for supplying the *P. aeruginosa* strain from a CF patient.

394

395 **Contributions**

396 Conceiving and designing the experiments: C. Cigana, A. Bragonzi, F. De Leo, G. Musco, M.E.
397 Bianchi. Performing the experiments: A. Rossi, I. De Fino, M. Melessike, F. De Leo, G. Quilici,
398 M.V. Mantonico, C. Fabris, F. De Marchis. Analysing the data: C. Cigana, A. Rossi, F. De Leo,
399 G. Quilici, F. De Marchis. Contributing reagents/materials/analysis tools: A. Bragonzi, G.
400 Musco, M.E. Bianchi. Writing the paper: A. Rossi, C. Cigana, A. Bragonzi, F. De Leo, G. Musco
401 and M.E. Bianchi.

402 **Consent for publication**

403 Not applicable

404 **References**

405 Andersson U, Ottestad W, Tracey KJ. Extracellular HMGB1: a therapeutic target in severe
406 pulmonary inflammation including COVID-19? Mol. Med. 2020 Dec 7;26(1):42.
407 Bianchi ME, Crippa MP, Manfredi AA, Mezzapelle R, Rovere Querini P, Venereau E. High-
408 mobility group box 1 protein orchestrates responses to tissue damage via inflammation, innate
409 and adaptive immunity, and tissue repair. Immunol. Rev. 2017 p. 74–82.
410 Bragonzi A. Murine models of acute and chronic lung infection with cystic fibrosis pathogens.

Int. J. Med. Microbiol. Urban & Fischer; 2010 Dec 1;300(8):584–93.

Bragonzi A, Paroni M, Nonis A, Cramer N, Montanari S, Rejman J, et al. Pseudomonas aeruginosa Microevolution during Cystic Fibrosis Lung Infection Establishes Clones with Adapted Virulence. Am. J. Respir. Crit. Care Med. 2009 Jul 15;180(2):138–45.

Chirico V, Lacquaniti A, Leonardi S, Grasso L, Rotolo N, Romano C, et al. Acute pulmonary exacerbation and lung function decline in patients with cystic fibrosis: High-mobility group box 1 (HMGB1) between inflammation and infection. Clin. Microbiol. Infect. 2015;

Choi HW, Tian M, Song F, Venereau E, Preti A, Park S-W, et al. Aspirin's Active Metabolite Salicylic Acid Targets High Mobility Group Box 1 to Modulate Inflammatory Responses. Mol. Med. 2015 Jan 18;21(1):526–35.

Chue P, Chue J. A review of olanzapine pamoate. Expert Opin. Pharmacother. 2012. p. 1661–70.

Cigana C, Lorè NI, Riva C, De Fino I, Spagnuolo L, Sipione B, et al. Tracking the immunopathological response to Pseudomonas aeruginosa during respiratory infections. Sci. Rep. 2016 Aug 17;6(1):21465.

Cigana C, Ranucci S, Rossi A, De Fino I, Melessike M, Bragonzi A. Antibiotic efficacy varies based on the infection model and treatment regimen for Pseudomonas aeruginosa. Eur. Respir. J. European Respiratory Society; 2020 Mar 1;55(3):1802456.

D'Agostino G, Cecchinato V, Uguccioni M. Chemokine Heterocomplexes and Cancer: A Novel Chapter to Be Written in Tumor Immunity. Front. Immunol. 2018 Sep 25;9:1–8.

Dominguez C, Boelens R, Bonvin AMJJ. HADDOCK: A protein-protein docking approach based on biochemical or biophysical information. J. Am. Chem. Soc. 2003;125(7):1731–7.

Döring G, Bragonzi A, Paroni M, Aktürk F-F, Cigana C, Schmidt A, et al. BIIL 284 reduces neutrophil numbers but increases P. aeruginosa bacteremia and inflammation in mouse lungs. J.

Cyst. Fibros. 2014 Mar;13(2):156–63.

Ekanayaka SA, McClellan SA, Peng X, Barrett RP, Francis R, Hazlett LD. HMGB1 Antagonist, Box A, Reduces TLR4, RAGE, and Inflammatory Cytokines in the Cornea of P. aeruginosa - Infected Mice. J. Ocul. Pharmacol. Ther. 2018 Dec;34(10):659–69.

Entezari M, Weiss DJ, Sitapara R, Whittaker L, Wargo MJ, Li J, et al. Inhibition of High-Mobility Group Box 1 Protein (HMGB1) Enhances Bacterial Clearance and Protects against Pseudomonas Aeruginosa Pneumonia in Cystic Fibrosis. Mol. Med. 2012 Mar 2;18(3):477–85.

Facchini M, De Fino I, Riva C, Bragonzi A. Long Term Chronic Pseudomonas aeruginosa Airway Infection in Mice. J. Vis. Exp. 2014 Mar 17;(85).

Gangemi S, Casciaro M, Trapani G, Quartuccio S, Navarra M, Pioggia G, et al. Association between HMGB1 and COPD: A Systematic Review. Mediators Inflamm. 2015;2015:1–8.

Haegens A, Vernooy JHJ, Heeringa P, Mossman BT, Wouters EFM. Myeloperoxidase modulates lung epithelial responses to pro-inflammatory agents. Eur. Respir. J. 2008 Feb 1;31(2):252–60.

Kilkenny C, Browne WJ, Cuthill IC, Emerson M, Altman DG. Improving Bioscience Research Reporting: The ARRIVE Guidelines for Reporting Animal Research. PLoS Biol. 2010 Jun 29;8(6):e1000412.

Krajewski M, Rothweiler U, D'Silva L, Majumdar S, Klein C, Holak TA. An NMR-based antagonist induced dissociation assay for targeting the ligand-protein and protein-protein interactions in competition binding experiments. J. Med. Chem. 2007;50(18):4382–7.

Kukavica-Ibrulj I, Facchini M, Cigana C, Levesque RC, Bragonzi A. Assessing Pseudomonas aeruginosa Virulence and the Host Response Using Murine Models of Acute and Chronic Lung Infection. Methods Mol. Biol. 2014. p. 757–71.

De Leo F, Quilici G, De Marchis F, Mantonico MV, Bianchi ME, Musco G. Discovery of 5,5′-Methylenedi-2,3-Cresotic Acid as a Potent Inhibitor of the Chemotactic Activity of the HMGB1·CXCL12 Heterocomplex Using Virtual Screening and NMR Validation. Front. Chem. 2020 Nov 26;8:1–17.

De Leo F, Quilici G, Tirone M, De Marchis F, Mannella V, Zucchelli C, et al. Diflunisal targets the HMGB1/CXCL12 heterocomplex and blocks immune cell recruitment. EMBO Rep. 2019 Oct 4;20(10):e47788.

Liou TG, Adler FR, Keogh RH, Li Y, Jensen JL, Walsh W, et al. Sputum biomarkers and the prediction of clinical outcomes in patients with cystic fibrosis. PLoS One. 2012;7(8).

Lu B, Antoine DJ, Kwan K, Lundbäck P, Wähämaa H, Schierbeck H, et al. JAK/STAT1 signaling promotes HMGB1 hyperacetylation and nuclear translocation. Proc. Natl. Acad. Sci. U. S. A. 2014;111(8):3068–73.

Mollica L, De Marchis F, Spitaleri A, Dallacosta C, Pennacchini D, Zamai M, et al. Glycyrrhizin Binds to High-Mobility Group Box 1 Protein and Inhibits Its Cytokine Activities. Chem. Biol. 2007 Apr;14(4):431–41.

Nazir I, Asim MH, Dizdarević A, Bernkop-Schnürch A. Self-emulsifying drug delivery systems: Impact of stability of hydrophobic ion pairs on drug release. Int. J. Pharm. 2019 Apr;561:197–205.

Neubig RR. Mind your salts: when the inactive constituent isn't. Mol. Pharmacol. 2010 Oct;78(4):558–9.

Rowe SM, Jackson PL, Liu G, Hardison M, Livraghi A, Solomon GM, et al. Potential role of high-mobility group box 1 in cystic fibrosis airway disease. Am. J. Respir. Crit. Care Med. 2008;178(8).

480 Schiraldi M, Raucci A, Muñoz LM, Livoti E, Celona B, Venereau E, et al. HMGB1 promotes
481 recruitment of inflammatory cells to damaged tissues by forming a complex with CXCL12 and
482 signaling via CXCR4. J. Exp. Med. 2012;209(3):551–63.
483 Song YH, Shin E, Wang H, Nolan J, Low S, Parsons D, et al. A novel in situ hydrophobic ion
484 pairing (HIP) formulation strategy for clinical product selection of a nanoparticle drug delivery
485 system. J. Control. Release. 2016 May;229:106–19.
486 Tomasello G, Armenia I, Molla G. The Protein Imager: a full-featured online molecular viewer
487 interface with server-side HQ-rendering capabilities. Elofsson A, editor. Bioinformatics. 2020
488 May 1;36(9):2909–11.
489 Veldkamp CT, Seibert C, Peterson FC, De La Cruz NB, Haugner JC, Basnet H, et al. Structural
490 basis of CXCR4 sulfotyrosine recognition by the chemokine SDF-1/CXCL12. Sci. Signal.
491 2008;1(37):1–10.
492 Vranken WF, Boucher W, Stevens TJ, Fogh RH, Pajon A, Llinas M, et al. The CCPN data model
493 for NMR spectroscopy: Development of a software pipeline. Proteins Struct. Funct. Bioinforma.
494 2005 Apr 6;59(4):687–96.
495 Waudby CA, Ramos A, Cabrita LD, Christodoulou J. Two-Dimensional NMR Lineshape
496 Analysis. Sci. Rep. 2016 Jul 25;6(1):24826.
497 Zhao P, Sharir H, Kapur A, Cowan A, Geller EB, Adler MW, et al. Targeting of the Orphan
498 Receptor GPR35 by Pamoic Acid: A Potent Activator of Extracellular Signal-Regulated Kinase
499 and β-Arrestin2 with Antinociceptive Activity. Mol. Pharmacol. 2010 Oct;78(4):560–8.
500 Van Zundert GCP, Rodrigues JPGLM, Trellet M, Schmitz C, Kastritis PL, Karaca E, et al. The
501 HADDOCK2.2 Web Server: User-Friendly Integrative Modeling of Biomolecular Complexes. J.
502 Mol. Biol. Academic Press; 2016 Feb 22;428(4):720–5.

Figures

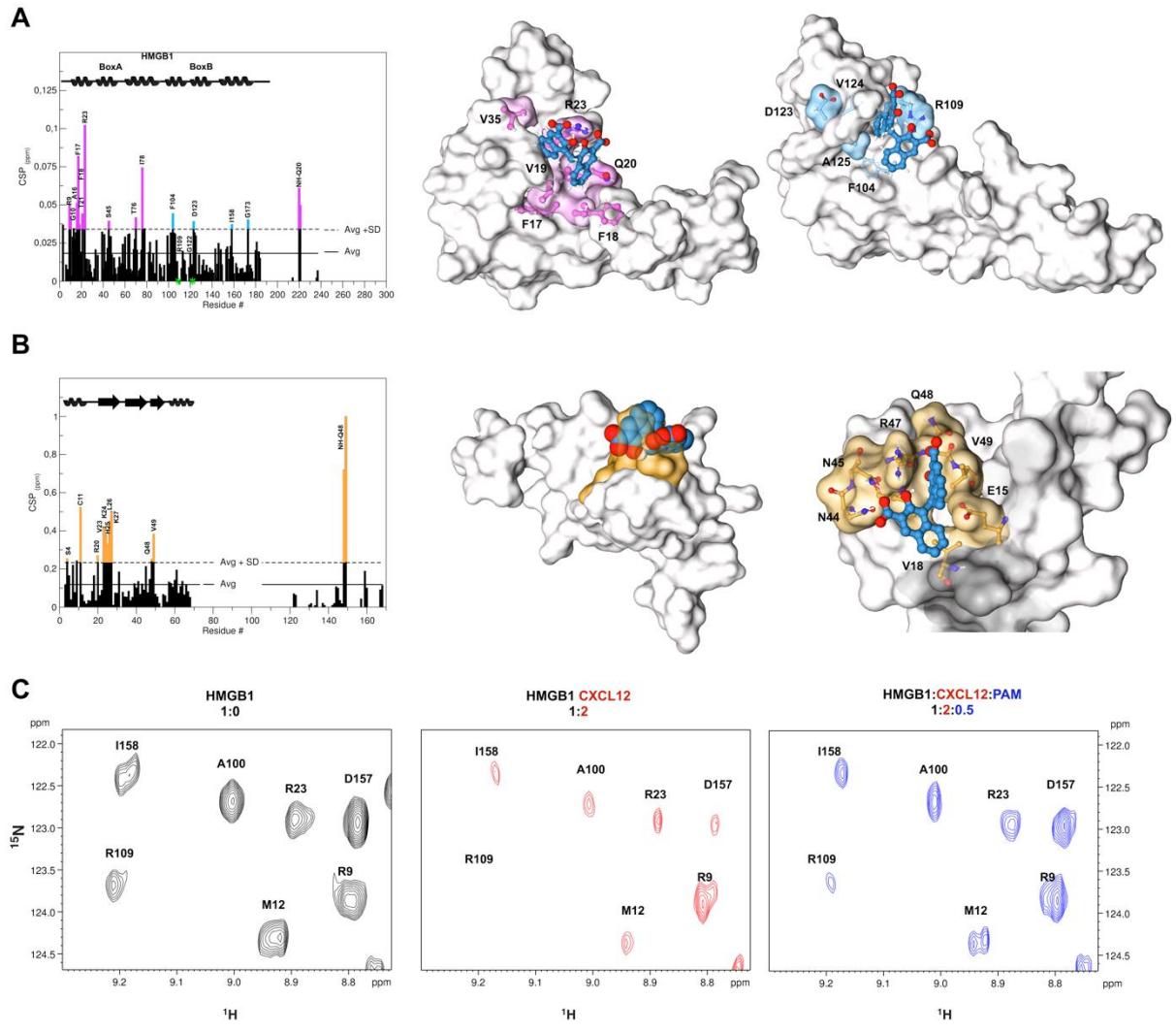

Figure 1. PAM directly binds to HMGB1 and CXCL12 and disrupts their heterocomplex

(A) Histogram showing residue-specific CSPs of ^{15}N-HMGB1 (~0.1 mM) upon addition of equimolar ratio of PAM (helices are schematically represented on top). Missing residues are prolines or are absent because of exchange with the solvent. BoxA and BoxB residues with CSP

> Avg + SD are represented in magenta and light blue, respectively. HADDOCK models of interaction of PAM (licorice representation) with BoxA (middle) and BoxB (right) (gray surface and colored residues with CSP > Avg + SD). HMGB1 residues (sticks) involved in hydrophobic and electrostatic interactions with PAM are labeled. **(B)** Histogram showing the CSPs of ^{15}N-CXCL12 amides (~0.1 mM) upon addition of equimolar ratio of PAM. Missing residues are prolines. Elements of secondary structure are represented on top. Middle: HADDOCK model of interaction of PAM (CPK representation) with CXCL12 (gray surface). CXCL12 residues with CSP > Avg + SD located around the sY21 binding site are in orange. Right: Zoom in the binding site, CXCL12 residues (sticks) involved in hydrophobic and electrostatic interactions with PAM (sticks) are explicitly labeled. **(C)** ^{1}H-^{15}N HSQC HMGB1 (0.1 mM) spectrum without (black, left), with 0.2 mM CXCL12 (red, middle) and upon addition of 0.05 mM PAM (blue, right).

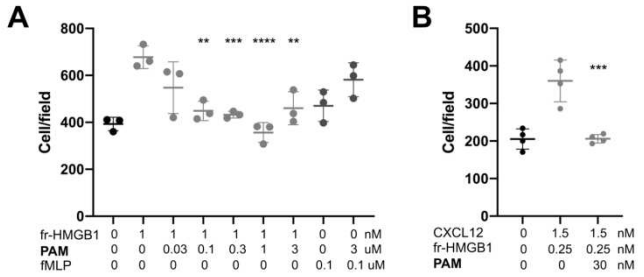

Figure 2. (A) PAM inhibits HMGB1-induced, but not fMLP-induced cell migration. Mouse 3T3 fibroblasts were subjected to chemotaxis assays in Boyden chambers, 1 nM fr- (fully reduced) HMGB1, or no chemoattractant was added in the lower chamber, together with the indicated concentrations of PAM. Data points with average ± standard deviation (Avg ± SD; n = 3, each point represents a biological replicate) in a representative experiment. Statistics: one-way ANOVA (P = 0.0001), followed by Dunnett's post-tests. **P < 0.0016, ***P < 0.0008, **** P <

0.0001 relative to no PAM addition. **(B)** PAM inhibits chemotaxis toward the HMGB1·CXCL12 heterocomplex. Data points (n = 3) with Avg ± SD in one representative experiment (of three performed in different days). Migration in the presence or absence of PAM is significantly different (P = 0.0002, one-way ANOVA plus Dunnett's post-test; ***P < 0.0004 relative to no PAM addition).

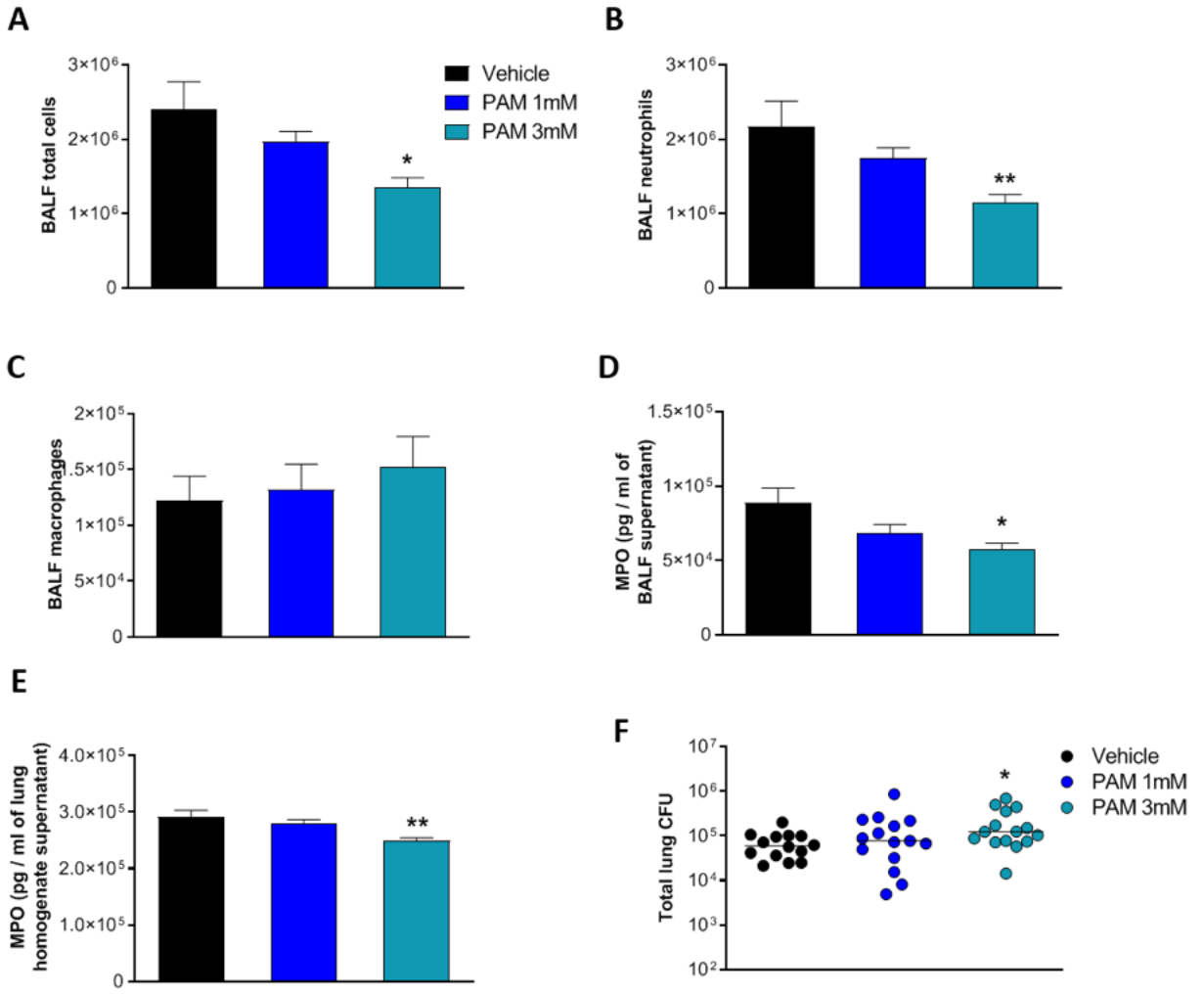

Figure 3. Efficacy of aerosol treatment with PAM (1 mM and 3 mM) in a mouse model of acute *P. aeruginosa* airway infection. C57BL/6NCrlBR male mice (aged 8–10 weeks) received intratracheal inoculation with 1×10^6 CFUs of planktonic PAO1 strain. Five minutes after

infection, PAM (1 mM, or 3 mM or vehicle) were administered *via* an aerosolizer. After six hours, mice were sacrificed, bronchoalveolar lavage fluid (BALF) was collected, and the lungs were excised and homogenized. Total cells (**A**), neutrophils (**B**) and macrophages (**C**) were counted on BALF. BALF and lung homogenates were centrifuged. MPO concentration was evaluated in the supernatants of BALF (**D**) and lung homogenate (**E**) by ELISA assay. Data are presented as mean ± SEM. BALF and lung homogenates were plated on tryptic soy agar to determine the bacterial burden (**F**). Each dot represents total CFUs per lung from one mouse, and horizontal lines represent the median values. Data are pooled from three independent experiments (n=14-15 mice). Statistical significance is indicated: * $p<0.05$; ** $p<0.01$.

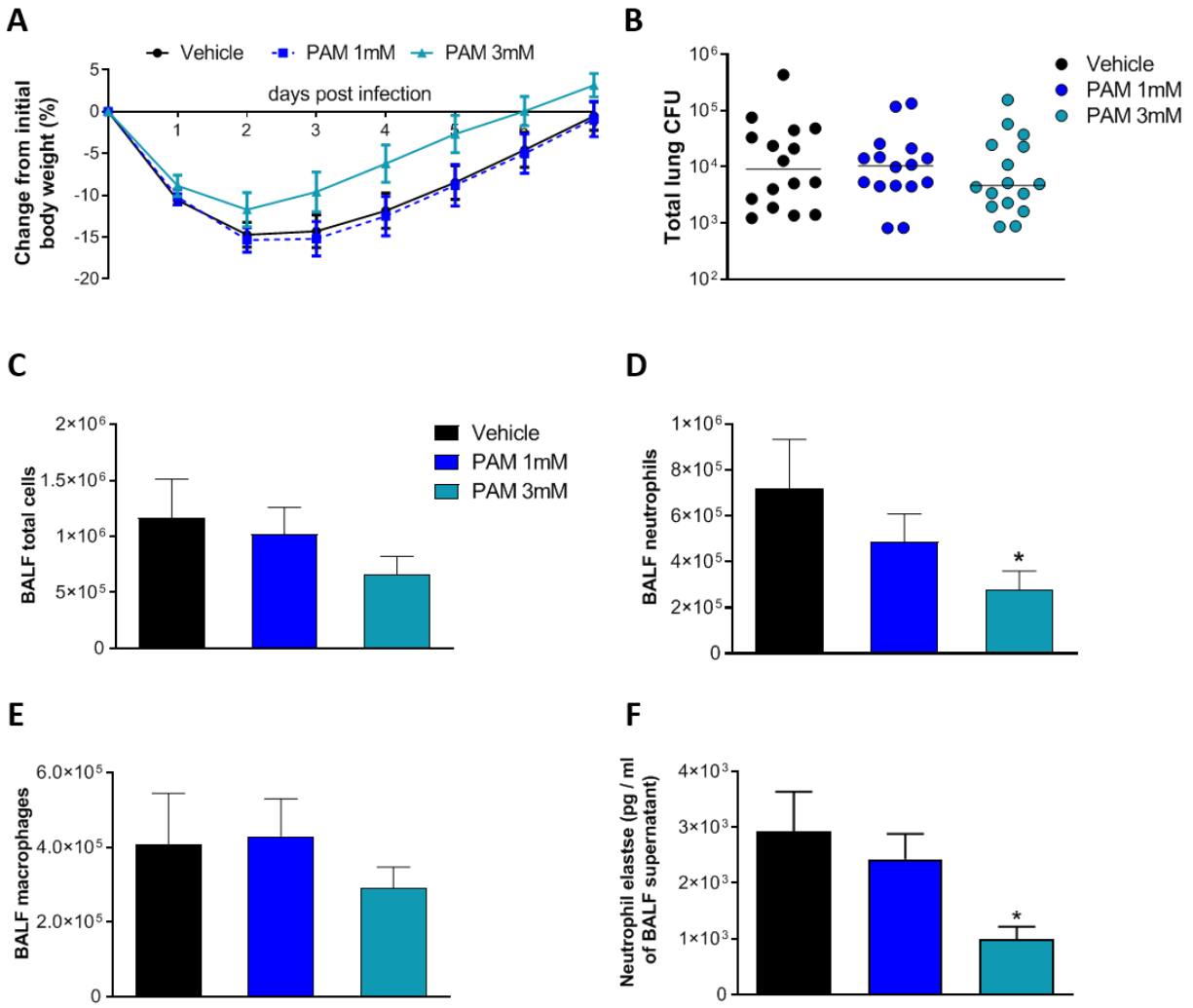

Figure 4. Efficacy of aerosol treatment with PAM (1 mM and 3 mM) in a murine model of *P. aeruginosa* MDR-RP73 chronic airways infection. C57BL /6NCrlBR male mice (aged 8–10 weeks) received intratracheal inoculation with 5×10^5 CFU of MDR-RP73 strain embedded in agar beads. Treatment started five minutes after infection, with PAM (1 mM and 3 mM) or vehicle administered *via* aerosol by Penn Century daily for seven days. Before each administration, mice were weighted, and the percentage change from the initial body weight was averaged for each group of mice (**A**). Data are presented as mean ± SEM. At day seven post-infection, mice were sacrificed, BALF was collected and lungs were excised and homogenized. BALF and lung homogenates were plated on tryptic soy agar to determine the bacterial burden (**B**). Each dot represents total CFU per lung from one mouse, and horizontal lines represent the median values. Total cell (**C**), neutrophil (**D**) and macrophage (**E**) counts were performed on BALF. Neutrophils elastase concentration was evaluated in the supernatants of BALF (**F**) by ELISA assay. Data are presented as mean ± SEM. Data are pooled from three independent experiments (n=15-16 mice). Statistical significance is indicated: * $p<0.05$.

Supplementary Files

This is a list of supplementary files associated with this preprint. Click to download.

- DeLeoetalSuppl.pdf